Breakup behavior of nanolayers in polymeric multilayer systems - Creation of nanosheets and nanodroplets

Jingxing Feng, Ziyou Zhang, Adrien Bironeau, Alain Guinault, Guillaume Miquelard-Garnier, Cyrille Sollogoub, Andrew Olah, Eric Baer

Breakup behavior of nanolayers in polymeric multilayer systems — Creation of nanosheets and nanodroplets

Jingxing Feng [a,*], Ziyou Zhang [a], Adrien Bironeau [b], Alain Guinault [b], Guillaume Miquelard-Garnier [b], Cyrille Sollogoub [b], Andrew Olah [a], Eric Baer [a]

[a] Center for Layered Polymeric Systems (CLiPS), Department of Macromolecular Science and Engineering, Case Western Reserve University, Cleveland, OH, 44106-7202, USA
[b] PIMM, UMR 8006, ENSAM, CNRS, CNAM, 151bd de l'Hôpital, 75013, Paris, France

A B S T R A C T

Multilayer films comprising polystyrene (PS)/polymethyl methalcrylate (PMMA) and PS/polycaprolatone (PCL) alternating nanolayers with varied layer thickness were fabricated by multilayer coextrusion. The nanolayers breakup phenomena of PMMA and PCL were characterized using atomic force microscopy (AFM), oxygen permeability, light transmission, wide-angle X-ray scattering (WAXS), and differential scanning calorimetry (DSC). The continuous layers started to break up into nanosheets and nanodroplets during the coextrusion process when the nominal layer thickness decreased to between 30 nm and 40 nm. Further decrease of the nominal layer thickness of PMMA and PCL resulted in less nanosheets and more nanodroplets. Oxygen permeability was effective for characterizing the onset thickness of layer breakup. The oxygen permeability for the PS/PCL system was modeled and demonstrated good correlation with estimated composition of continuous layers, nanosheets, and nanodroplets.

Keywords:
Multilayer coextrusion
Layer breakup
Polymer nanodroplets

1. Introduction

Forced assembly by multilayer coextrusion was proven by Dow Chemical to be a reliable technique for producing nanolayers and microlayers in a continuous process [1]. The past two decades witnessed the rapid development of multilayer coextrusion which evolved from uniform layers to gradient layers, from one-dimensional structure to two-dimensional structure and from two-component systems to more complex systems [2]. The nano/microlayered films demonstrated highly tunable gas barrier [3], mechanical [4], optical [5,6] and electrical [7,8] properties arising from scaling and layer-layer interaction.

For many polymer multilayer systems, there existed a layer thickness below which the polymer layers lost their integrity. In these cases, the polymer layers break and transform into nanosheets and nanodroplets, similar to the dewetting phenomenon observed in thin films [9,10]. Such nanostructures were observed on several polymer pairs (polypropylene (PP)/polyethylene oxide (PEO) [11], polycarbonate (PC)/polyethylene terephthalate (PET) [12], PP/polystyrene (PS) [13] or PS/polymethyl methacrylate (PMMA) [14]). As such, the critical layer thickness was defined in a recent work by Sollogoub et al. as the smallest continuous layer observed in a given multilayer system, where they systematically studied the breakup behavior of nanolayers during coextrusion process of PS/PMMA [10,14]. They observed that this critical layer thickness was close to 7 nm for polystyrene and 10 nm for PMMA regardless of the processing route; suggesting it depends only on material parameters. It was speculated this critical layer thickness is due to small interfacial perturbations that are amplified by van der Waals disjoining forces that become dominant over stabilizing interfacial tension forces for thicknesses on the order of 10 nm.

In 2005, Baer et al. benefited from layer break-ups in nanolayered films to develop nanodroplets as polymer blends morphologies [12–14]. The nanolayered films were prepared from coextrusion and then thermally treated at high temperature. Even though the multilayer films had stable morphology at room temperature, the nanolayers were unstable at high temperature. The polymer nanodroplets were generated from the breakup and coalescence of nanolayers during thermal treatment. High density polyethylene and polypropylene were both made into well-dispersed nanodroplets in a PS matrix using this approach [15,16]. It was discovered that the size of the nanodroplets could be

* Corresponding author.
E-mail address: jxf309@case.edu (J. Feng).

controlled by changing the layer thickness of films before thermal treatment [15,17]. Thermal treatment of thicker films yielded larger nanodroplets and thinner films produced smaller nanodroplets.

In this paper, the possibility of using a macroscopic analysis technique, oxygen permeability measurement, to track breakup phenomenon of polymer nanolayers was investigated, using two different multilayer systems: glassy/glassy (PS/PMMA) and glassy/semi-crystalline (PS/polycaprolactone (PCL)). The multilayer composite films with different nominal layer thicknesses were prepared by varying the layer number and polymer compositions. When the layer thickness was lower than the thickness at which the layers start to break (onset thickness for layer break-up) nanosheets and nanodroplets were directly formed during the coextrusion process (as opposed to the nanodroplets formerly produced from the annealing of continuous multilayer films [16,17,21]). Oxygen permeability and light transparency of the composite films were performed on the extruded films and revealed the layer breakups in both systems. Coupling these measurements with an in-depth morphological analysis of the PCL (via AFM, Wide-angle X-ray scattering, Differential Scanning Calorimetry and optical light transmission), we showed that it was possible to model the effective oxygen permeability of PCL to quantitatively obtain the ratio of nanosheets and nanolayers in the PS/PCL films.

2. Materials and methods

2.1. Materials

The polystyrene (PS) used in this study was supplied by Americas Styrenics LLC (MC3650). It had a glass transition temperature of 95 °C and melt flow index of 13.0 g/10 min measured at 200 °C under a load of 5 kg. The poly (methyl methacrylate) (PMMA) was a poly (methyl methacrylate-co-ethyl acrylate) which contained 5%–10% ethyl acrylate to prevent depolymerization during extrusion, purchased from Arkema (Plexiglas VS). The glass transition temperature (T_g) of the PMMA was measured as 95 °C (due to the presence of ethyl acrylate in the PMMA) and its melt flow index was 27.0 g/10 min measured at 230 °C/3.8 kg. The polycaprolactone (PCL) was acquired from Perstorp (CAPA 6800). Its melting temperature, glass transition temperature, and crystallization temperature respectively were measured as 58 °C, −60 °C, and 35 °C. The melt flow index of PCL was 2.4 g/10 min measured at 160 °C under a load of 2.16 kg. The materials' information is shown in Table 1.

The melt viscosity of PS, PMMA and PCL was determined as a function of temperature using a Kayeness Galaxy 1 melt flow indexer at a shear rate of 10 s^{-1}. The extrusion temperature was selected to ensure the polymeric material's rheological compatibility for extrusion and to maximize layer uniformity. Before the coextrusion process, the PMMA was dried in a vacuum oven for 24 h at 80 °C. The PCL was dried for 48 h at 40 °C. Films with 513 and 2049 alternating PS/PMMA and PS/PCL layers were produced through continuous coextrusion process [23,24]. The composition of the films in volume was changed to vary the individual layer thickness. The extruder and layer multiplication elements were 200 °C and the 14-inch exit die temperature was 190 °C. The takeoff temperature of the chill roll was 60 °C. A sacrificial polyethylene skin layer was coextruded with the PS/PMMA, PS/PCL multilayers. The skin layer was peeled off before characterization. Other parameters of the coextrusion process were identical to previous setups.

Table 1
Properties of materials for coextrusion process.

Materials	Trade Name	T_m (°C)	T_g (°C)	T_c (°C)	Density (g/cm^3)	Refractive Index
PS	AmSty MC3650	–	95	–	1.04	1.58
PMMA	Arkema Plexiglas VS	–	95	–	1.18	1.49
PCL	Perstorp CAPA 6800	58	−60	35	1.14	1.48

2.2. Atomic force microscopy

The extrusion direction morphologies of the as-extruded films were characterized by atomic force microscopy (AFM). The film was embedded in epoxy (Loctite Heavy Duty Epoxy, Loctite Inc.) and cured at room temperature for 24 h. The film cross-sections were prepared perpendicular to the extrusion direction at −100 °C (for PS/PCL system) and −80 °C (for PS/PMMA system) by an ultramicrotome equipped with a cryogenic chamber (Leica EM UC7, Leica Microsystems). The height variance of the samples after microtoming was controlled to be less than 30 nm. The AFM images were acquired at room temperature in air with a scanning probe microscope (Nanoscope IIIa, Digital Instruments, Santa Barbara, CA) operated in the tapping mode. A rectangular type silicon tapping mode probe was used to record height and phase images simultaneously. The tip radius was 10 nm and the spring constant was 50 N/m with a resonance frequency of around 320 kHz. To acquire high-quality images of the layered morphology and to capture the breakup behavior of the PMMA layers, a low scan rate was used for AFM. The number of layers, nanosheets, and nanodroplets were counted from at least three AFM scans with a size of 10 μm by 10 μm. The areas for imaging were randomly selected from the cross-section. If the layers were continuous throughout the 10 μm image, the layer was defined as a continuous layer. Otherwise, the layer was defined as a breakup layer.

2.3. Oxygen permeability

Oxygen flux $J(t)$ at 0% relative humidity, 1 atm, and 23 °C was measured with a MOCON OX-TRAN 2/20. Permeability was calculated from the steady flux J_0 according to Equation (1).

$$P(O_2) = J_0 l / \Delta p \tag{1}$$

where Δp is the oxygen pressure drop and l is the film thickness. The permeability values in this work were reported in Barrer. One Barrer is equivalent to 10^{-10} (cm^3 O_2) cm cm^{-2} s^{-1} $cmHg^{-1}$.

Oxygen permeability of the film was affected by both polymer phases. For example, in the case of the PS/PCL system, the effective PCL permeability could be calculated using Equation (2) as follows,

$$\textit{Film Permeability} = \left(\frac{V_{PCL}}{P_{PCL}} + \frac{V_{PS}}{P_{PS}}\right)^{-1} \tag{2}$$

where V_{PCL} and V_{PS} were the volume fraction of PCL and PS in the film.

Similarly, the effective PCL permeability consisted of the permeability of the PCL layers, nanosheets, and nanodroplets as shown in Equation (3). The modeling of oxygen permeability will be discussed later in this paper.

$$P_{PCL} = \left(\frac{V_{PCL\ Layers}}{P_{PCL\ Layers}} + \frac{V_{PCL\ Sheets}}{P_{PCL\ Sheets}} + \frac{V_{PCL\ Droplets}}{P_{PCL\ Droplets}}\right)^{-1} \tag{3}$$

where $V_{PCL\ Layers}$ and $V_{PCL\ Sheets}$ and $V_{PCL\ Droplets}$ were the volume fraction of PCL layers, nanosheets, and nanodroplets.

2.4. Optical transmission

The transparency of the as-extruded films at varied wavelengths was measured using a UV/Visible spectrometer (Lambda 1050) in transmission mode. Details of light transmission measurement setup was discussed in the previous paper [25]. The sacrificial skin layer was peeled off before the sample was measured with the UV/Visible spectrometer.

2.5. Wide-angle X-ray scattering

The wide-angle X-ray scattering (WAXS) system setup has been presented in details in a previous publication [26]. Briefly, it consisted in an X-ray generator (sealed-tube, fine point Cu Kα filtered source operating at 30 kV and 30 mA, $\lambda = 1.54$ Å), a computer-controlled wide-angle goniometer, and an imaging plate as a detector. The X-ray beam was aligned in extrusion direction of the samples. The samples were prepared from a stack of up to 10 films. The exposure time in the X-ray beam was 12 h for each sample. The WAXS patterns were collected by an imaging film which was read from an image plate reader (Fujifilm FDL5000).

2.6. Differential scanning calorimetry

The heating thermograms were recorded by a differential scanning calorimeter (TA Q2000 TA Instruments Inc., New Castle, DE). The as-extruded films were dried in a desiccator at room temperature for 48 h before DSC measurement. The specimens were prepared by loading 4–8 mg of the as-extruded films into aluminum pans. The temperature range was 10 °C to 90 °C. The heating rate was 10 °C/minute.

3. Results and discussion

Fig. 1 showed the morphology of as-extruded PS/PMMA films. The PS phase was the dark color phase and the PMMA one the light color one in AFM phase images, as identified with varying PS/PMMA proportions in the films. Both PS and PMMA were continuous layers when the nominal layer thickness was 60 nm. At 20 nm nominal layer thickness, about half of the layers remain continuous as shown in the AFM images. Some PMMA layers broke up into elongated nanosheets which were parallel to the continuous layers. The rest of the layers broke up into nanodroplets. The nanodroplets were less elongated and had lower aspect ratios compared with the nanosheets. The fact that some layers broke up while others remained continuous was due to the variation in single layer thickness of the alternating layers during the multilayer coextrusion process. The minimum thickness for continuous layers was observed to be 20 nm. In addition, it was observed that the thickness of the continuous layers varied at different locations. The unstable continuous layers were precursors of pending breakup and would finally break into nanosheets when the layer thickness was further decreased. At 10 nm nominal layer thickness, as shown in Fig. 1c, more layers broke up into nanosheets and more nanodroplets were observed. At 5 nm nominal layer thickness shown in Fig. 1d, no continuous layers existed across the film. It was evident, based on AFM morphology, that the nanosheets and nanodroplets were still aligned in the layer direction, even when some of the nanodroplets coalesced into larger droplets.

Fig. 2 illustrated the morphology of as-extruded PS/PCL films. In this system, since PS was the material with higher modulus, it showed as the light color phase and PCL showed as the dark color phase. The breakup behavior of the PS/PCL system was similar to that of the PS/PMMA system. As layer thickness decreased, the nanolayers experienced a gradual breakup process. The critical layer thickness (as defined by Sollogoub et al. [14]) for PMMA in the PS/PMMA system and PCL in the PS/PCL system was close to 20 nm, which is similar (though a bit higher) than what has been observed in the paper [14].

The sizes of the nanodroplets observed in Figs. 1d and 2d were collected from a series of AFM phase images for each sample. The difference between nanosheets and nanodroplets was set by their aspect ratios. The broken layers that have an aspect ratio larger than 10:1 were defined as nanosheets. The broken layers that have an aspect ratio smaller than 10:1 were defined as nanodroplets. By this definition, the statistics for the nanodroplets size and size distribution were collected and demonstrated in Fig. 3. As shown in Fig. 3, the PMMA nanodroplets had a mean droplet size of around 100 nm and PCL nanodroplets had a mean droplet diameter of around 150 nm. The slight difference in droplet size distribution could be explained by the material properties. PMMA is a glassy polymer with a glass transition temperature of 95 °C. PCL is a semi-crystalline polymer with a crystallization temperature of 35 °C. It could be expected that the layer breakup process took place during the polymer flow as it exited the film die. The coalescence of the nanodroplets took place during the cooling of the polymer films after breaking up. Compared with PCL, the PMMA nanodroplets had less time to coalesce because of its high T_g, and therefore have smaller sized droplets.

Oxygen permeability for PS/PMMA and PS/PCL films was measured in order to predict the breakup behavior. The effective PMMA oxygen permeability was plotted against the PMMA nominal thickness as shown in Fig. 4. The nominal thickness was calculated from total film thickness, number of layers and composition. For continuous layers, the nominal thickness reflected quantitatively the measured layer thickness of PMMA layers. In the breakup layers, we used the nominal thickness of PMMA implied prior to breakup. The effective PMMA oxygen permeability was calculated on the basis of series model which assumes that the PS layers and PMMA layers were both continuous and parallel. Thus, for the amorphous-amorphous PS/PMMA multilayer system whose oxygen permeability was constant with changing layer thickness, the effective PMMA oxygen permeability was supposed to be constant as well. It remained constant until the nominal layer thickness decreased to 30 nm. However, due to layer breakup phenomenon, the effective PMMA oxygen permeability decreased when the nominal layer thickness decreased below the critical layer thickness of PMMA prior to layer breakup. The PMMA nanosheets and nanodroplets did not provide an oxygen barrier as effectively as the continuous layers. As a result, the effective PMMA oxygen permeability was higher when layers broke up. The difference between the effective PMMA oxygen permeability at 30 nm nominal thickness and that of neat PMMA films was close to 20%. Then, since the PMMA nanodroplets had higher oxygen permeability than the PMMA nanosheets, the effective PMMA oxygen permeability increased gradually with the decrease of PMMA nominal layer thickness. As shown in Fig. 4, the effective PMMA oxygen permeability kept increasing as more layers broke up and more nanosheets coalesced into nanodroplets. The effective PMMA oxygen permeability increased to six times the oxygen permeability of PMMA neat films when the PMMA consisted mainly of nanodroplets.

The effective PCL oxygen permeability was plotted in Fig. 5. The change of effective PCL oxygen permeability was different from and more complicated than the PMMA oxygen permeability in the PS/PMMA system. The PCL permeability of 20,000 nm represents the permeability of neat PCL films showing an oxygen permeability of 1.0 Barrer. The oxygen permeability decreased with the decrease of the PCL layer thickness due to the effect of confined crystallization. The crystal morphology of PCL changed from spherulites to stacked

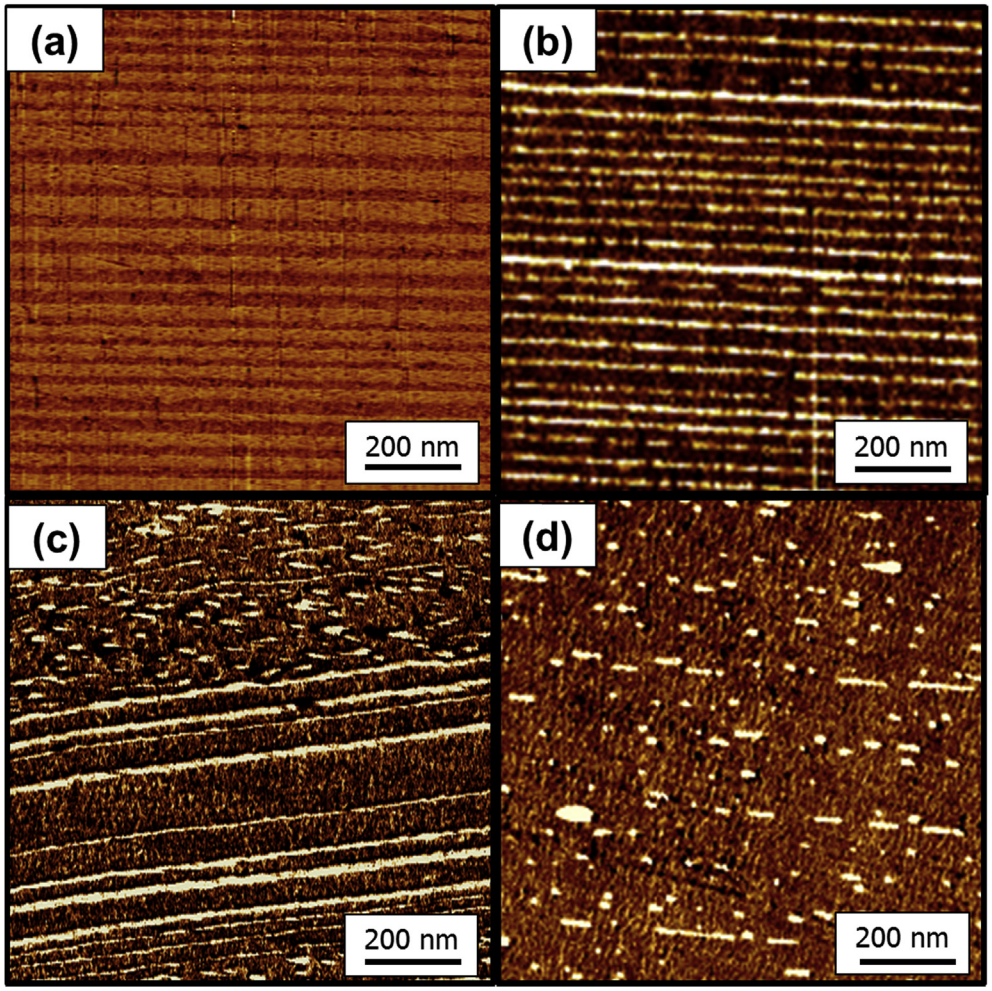

Fig. 1. Extruded-direction AFM phase morphologies of 513 layer PS/PMMA as-extruded films. The light color phase in the figure is PMMA and the dark color phase is PS. (a) Composition: 50% PMMA, 50% PS, nominal PMMA layer thickness = 60 nm; (b) Composition: 20% PMMA, 80% PS, nominal PMMA layer thickness = 20 nm; (c) Composition: 10% PMMA, 90% PS, nominal PMMA layer thickness = 10 nm; (d) Composition: 5% PMMA, 95% PS, nominal PMMA layer thickness = 5 nm. (For interpretation of the references to color in this figure legend, the reader is referred to the Web version of this article.)

lamellae when the thickness was decreased to around 1 μm [23]. The oxygen permeability continued to decrease with the decrease of nominal thickness due to the decrease in the number of lamellar layers in the PCL phase. Therefore, oxygen molecules took a more tortuous path when traveling through layers of PCL lamellae. This result coincided with the confined crystallization theory discussed in a previous paper [23]. The PCL oxygen permeability reached its minimum when the layer thickness was in the range of 40 nm−100 nm and having a permeability of 0.010 Barrer. The oxygen permeability of PS remained constant with varying layer thickness at 2.2 Barrer. PS contribution to the oxygen barrier properties was insignificant when the PCL was in lamellar morphology. When the PCL layer thickness was below 30 nm, the oxygen permeability increased significantly indicating layer breakup. The threshold of layer breakup could be identified as the nominal layer thickness where the PCL oxygen permeability started to increase and in this case that was 30 nm. The oxygen permeability continued to increase as more and more PCL broke up into nanosheets and nanodroplets. The PCL nanosheets and nanodroplets did not provide as good an oxygen barrier as continuous layers because of two factors. The first was the physical breakup of layers which enabled oxygen molecules to pass through easily. The second factor was crystallinity (decreased crystallinity and modified orientation). The nanosheets and nanodroplets had much higher oxygen permeability than the more crystalline PCL continuous Nevertheless, the films containing mostly nanodroplets and nanosheets still had superior oxygen barrier properties than PCL control films. We found that this was the case when the nanodroplets and nanosheets were elongated perpendicular to the extrusion direction as well as having lamellar crystalline structure perpendicular to the film surface. It could be predicted that the elongated nanosheets had lower oxygen permeability than spherical nanodroplets since the nanosheets had larger aspect ratios working as platelet fillers to bar oxygen molecules.

The oxygen permeability measurement was combined with the AFM morphological study to generate a model to calculate the number of continuous layers, nanosheets, and nanodroplets. The contribution of each of the three components was taken into consideration when calculating the overall effective PCL permeability. The number of continuous layers, nanosheets, and nanodroplets was obtained from statistics derived from AFM images as shown in Table 2. With 60 nm PCL nominal thickness, the PCL phase was all continuous layers. With 3 nm and 5 nm nominal PCL thicknesses, the samples contained only nanosheets and nanodroplets and no continuous layer was observed. The films with thickness in between contained all three morphologies according

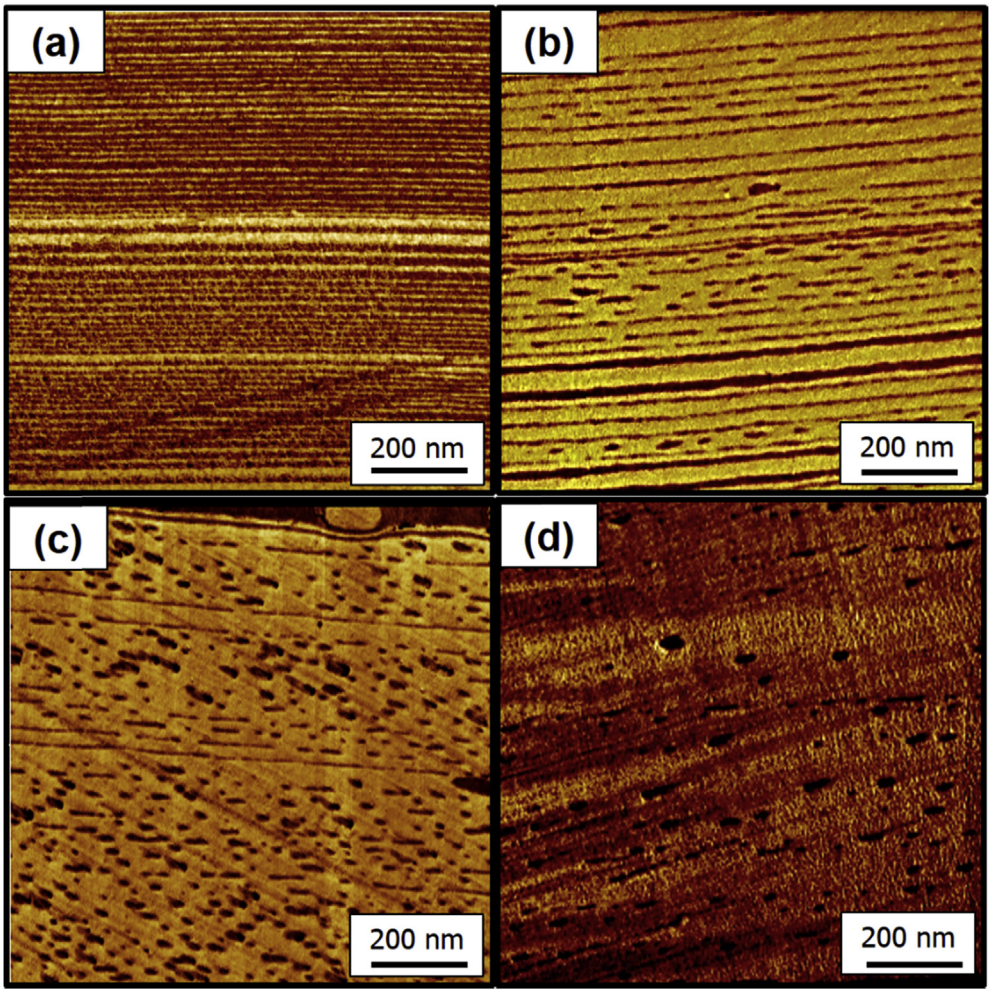

Fig. 2. Extruded-direction AFM phase morphologies of 513 layer PS/PCL as-extruded films. The light color phase in the figure is PS and the dark color phase is PCL. (a) Composition: 50% PCL, 50% PS, nominal PCL layer thickness = 60 nm; (b) Composition: 20% PCL, 80% PS, nominal PCL layer thickness = 20 nm; (c) Composition: 10% PCL, 90% PS, nominal PCL layer thickness = 10 nm; (d) Composition: 5% PCL, 95% PS, nominal PCL layer thickness = 5 nm. (For interpretation of the references to color in this figure legend, the reader is referred to the Web version of this article.)

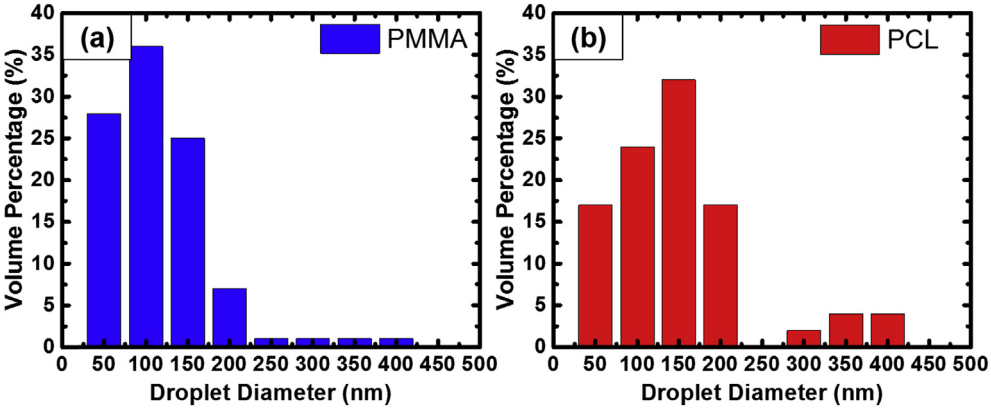

Fig. 3. Size distribution of nanodroplets prepared from layer breakup. (a) Composition: 5% PMMA, 95% PS, nominal PMMA layer thickness = 5 nm; (b) Composition: 5% PCL, 95% PS, nominal PCL layer thickness = 5 nm.

to AFM phase images shown in Fig. 2. In Table 2, the total number of discontinuous layers includes the addition of the amount of nanosheets and nanodroplets. The minimum continuous layer thickness was the thickness of the thinnest layer observed among all AFM images.

The oxygen permeability of continuous PCL layers was measured as 0.010 Barrer while the oxygen permeability of PCL nanosheets and PCL nanodroplets is unknown. The eight data

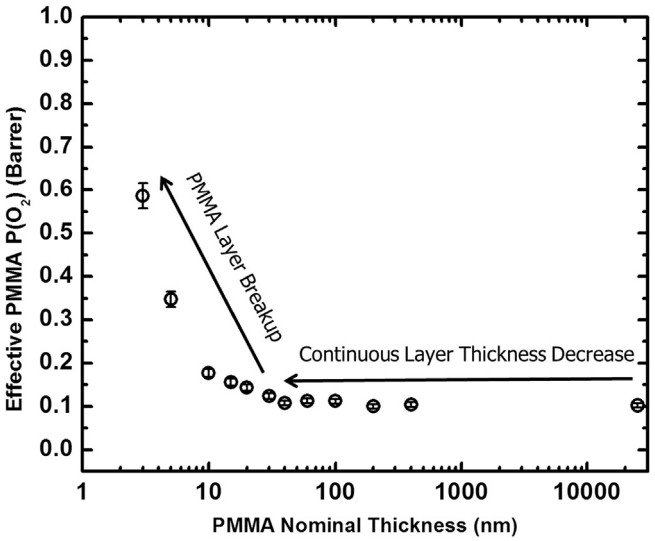

Fig. 4. Effective PMMA oxygen permeability in PS/PMMA multilayer films.

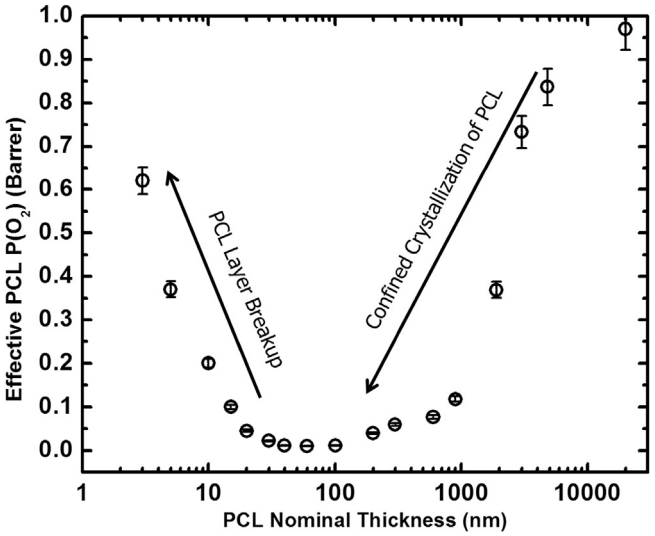

Fig. 5. Effective PCL oxygen permeability in PS/PCL multilayer films.

points in Table 2 were used to fit oxygen permeability of PCL nanosheets and PCL nanodroplets using equation (3). The result showed that the oxygen permeability of PCL nanosheets was 0.090 Barrer and the oxygen permeability of PCL nanodroplets was 1.0 Barrer. The modeled effective oxygen permeability of PCL was calculated using the fitting results and plotted as shown in Fig. 6. The oxygen permeability model demonstrated a good fit over the

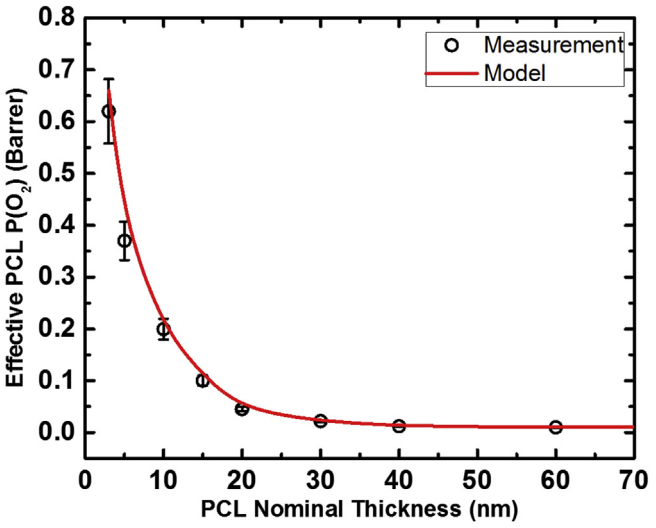

Fig. 6. Comparison of modeled PCL oxygen permeability and measure oxygen permeability.

measured effective PCL oxygen permeability. As a result, the oxygen permeability of the nanosheets and nanodroplets reflected that the nanosheets were nine times higher in oxygen permeability compared to continuous layers while the nanodroplets permeability was similar to neat PCL films in terms of oxygen barrier.

Fig. 7 illustrated the optical light transmission in the visible wavelength range for as-extruded PS/PMMA and PS/PCL films. The light transmission was measured to investigate the domain size of the nanosheets and nanodroplets. The PS/PMMA system showed high transparency with thickness ranging from 5 to 30 nm. Since the refractive index contrast for PS ($n = 1.58$) and PMMA ($n = 1.49$) was 0.09, the composite films would show visible light absorption when the PMMA domain size was larger than 100 nm. However, the data in Fig. 7a showed high transparency for visible light indicating that most of the PMMA domains were smaller than 100 nm in diameter. This result was consistent with the AFM image (Fig. 1) and the nanodroplet statistics shown in Fig. 3a. In terms of the PS/PCL system, due to the fact that PCL is a semicrystalline material, the PS/PCL composite films were translucent. The light scattering was caused by the refractive index contrast between crystal and amorphous domains of PCL. As shown in Fig. 7b, the transparency of the PS/PCL system increased with the decrease of nominal PCL layer thickness which implies that the light scattering of PCL was reduced. Two factors contributed to the light scattering reduction of the PCL phase. On the one hand, while breaking up from continuous layers to nanosheets and nanodroplets, the PCL layers lost its continuity and the light could pass through the film without being scattered by PCL. On the other hand, the crystalline domains in PCL nanodroplets were smaller and finer than

Table 2
Modeling of PCL oxygen permeability. The number of continuous layers, nanosheets, and nanodroplets was calculated from statistics derived from AFM phase images.

PCL Nominal Layer Thickness (nm)	Continuous Layers (%)	Nanosheets (%)	Nanodroplets (%)	Total Discontinuous Layers (%)	Minimum Continuous Layer Thickness (nm)
60	100	0	0	0	30
40	80	15	5	20	20
30	40	45	15	60	20
20	18	35	47	82	20
15	5	30	65	95	20
10	2	20	78	98	20
5	0	15	85	100	N/A
3	0	5	95	100	N/A

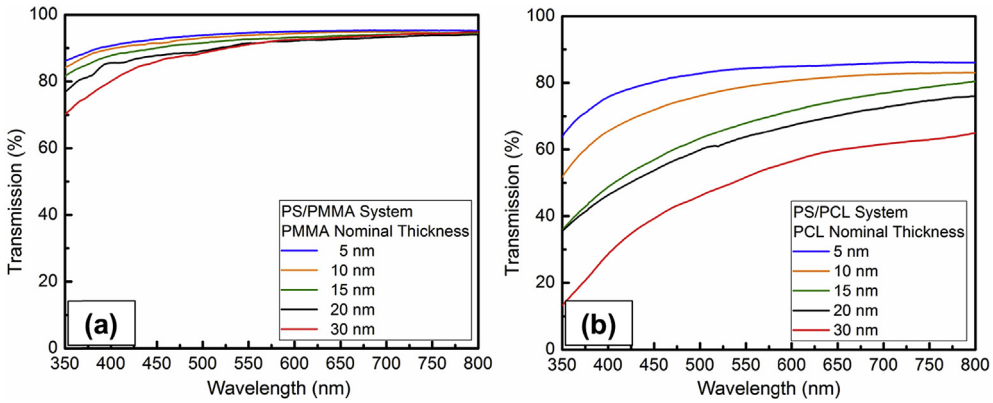

Fig. 7. Visible light transmission of 513-layer PS/PMMA and PS/PCL films. The composition was 80% PS and 20% PMMA or PCL. (a) PS/PMMA system; (b) PS/PCL system.

those in PCL continuous layers. The size decrease of PCL crystal domains could give rise to increase of transparency due to decrease of the number of scattering interfaces.

Fig. 8 presented the scattering pattern of as-extruded PS/PCL films in extrusion direction. Typical PCL crystals exhibit scattering pattern with high intensity at 17° and 22° representing PCL (110) and PCL (200). Fig. 8a showed the strong in-plane orientation of PCL where the scattering patterns were condensed at 90° and 270° azimuth. This result was consistent with previous work by Ponting et al. [23] PS/PCL films containing nanosheets and nanodroplets also demonstrated strong scattering patterns indicating that the nanosheets and nanodroplets were crystalline and exhibited in-

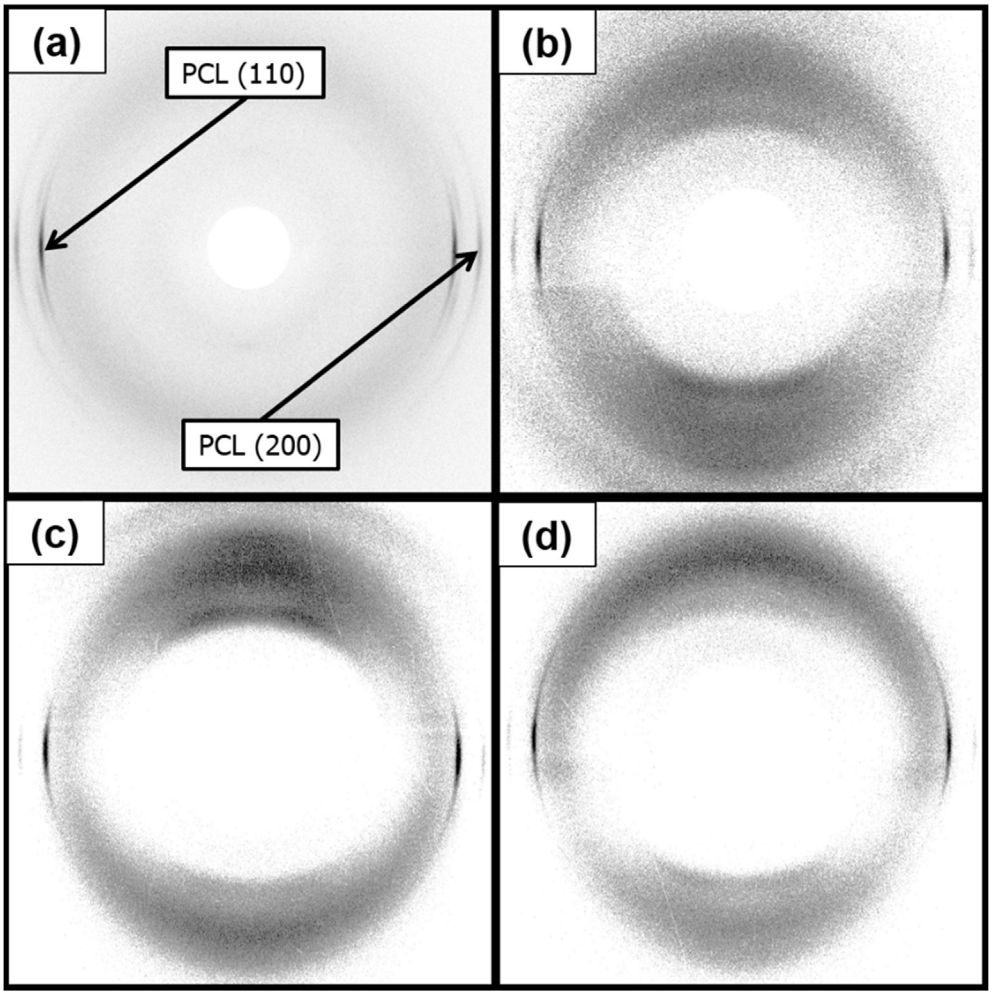

Fig. 8. Extrusion-direction wide-angle X-ray scattering pattern of 513 layer PS/PCL as-extruded films. (a) Composition: 50% PCL, 50% PS, nominal PCL layer thickness = 60 nm; (b) Composition: 20% PCL, 80% PS, nominal PCL layer thickness = 20 nm; (c) Composition: 10% PCL, 90% PS, nominal PCL layer thickness = 10 nm; (d) Composition: 50% PCL, 50% PS, nominal PCL layer thickness = 5 nm.

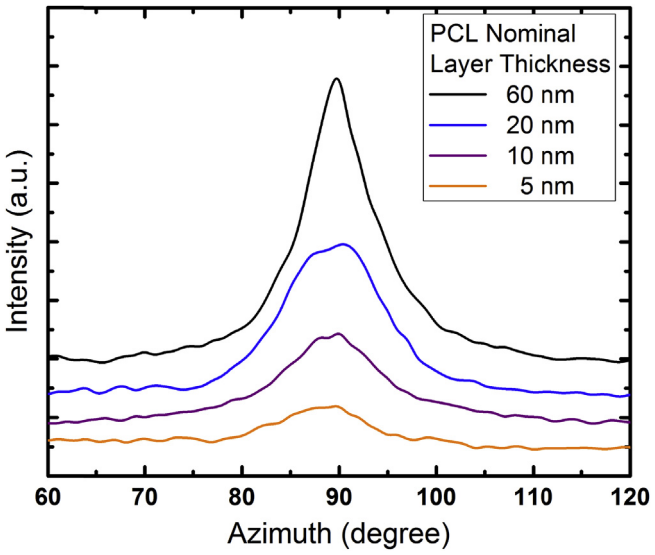

Fig. 9. Azimuthal plot of WAXS at $2\theta = 17^{\circ}$ of 513 layer PS/PCL as-extruded films.

plane orientation crystal structure.

Fig. 9 showed the azimuthal plot of WAXS data at $2\theta = 17^{\circ}$ representing the crystal orientation of PCL (110). The sharpest peak was the 60 nm samples with all continuous PCL layers. The PCL was considered to have in-plane lamellae structure. With the decrease of layer thickness, the relative intensity of peak versus background decreased indicating a reduction in in-plane orientation. This result implied that broken up PCL layers partially maintained in-plane lamellae structure with a decrease of crystal orientation. We compared nominal 10 nm films with nominal 5 nm films consisting mostly of nanodroplets. Neither sample contained continuous layers but the 10 nm films demonstrated larger relative peak intensity. One could postulate that the nanosheets had stronger in-plane orientation than nanodroplets.

The azimuthal intensity distribution of PCL (110) reflection from the WAXS pattern was analyzed to obtain the Hermans orientation function after subtraction of the amorphous contribution [27]. The orientation function f_{110} was calculated as

$$f_{110} = \frac{3\langle \cos^2 \phi_{110} \rangle - 1}{2} \tag{4}$$

where

$$\cos^2 \phi_{110} = \frac{\int_0^{\pi/2} I_{110}(\phi) \cos^2 \phi \sin \phi \mathrm{d}\phi}{\int_0^{\pi/2} I_{110}(\phi) \sin \phi \mathrm{d}\phi} \tag{5}$$

and $I_{110}(\phi)$ was the corrected scattering intensity of the PCL (110) reflection at the azimuth ϕ [23]. If the Hermans orientation function is equal to 1, the polymer chains were perpendicular to the polymer layers; if the Hermans orientation function is equal to 0, the PCL had random orientation. The calculated values of PCL in PS/PCL films were shown in Table 3. For PS/PCL films with 60 nm nominal layer thickness, the Hermans orientation function is 0.8 which was close to the value reported in the previous work [23]. It indicated that the PCL layers had strong in-plan orientation. When the nominal layer thickness was decreased to 20 nm, 10 nm, and 5 nm, f_{110} decreased to 0.55, 0.22, and 0.12 respectively indicating weaker orientation of PCL in nanosheets and nanodroplets. The film with 5 nm nominal PCL layer remained some in-plane orientation due to scattering of PCL chains in the elongated nanodroplets.

Fig. 10 presented the melting behavior of PCL in as-extruded PS/PCL films and the crystallinity calculation results were listed in Table 3. The onset temperature of PCL melting was 40 °C and the peak temperature was 58 °C which was constant with PCL control films. The crystallinity of PCL was calculated using 135.5 J/g as the enthalpy to melt PCL crystals [28]. The crystallinity of PCL control films was measured to be 49%. The crystallinity of 60 nm PCL layers was much lower than the PCL control films due to the effect of confined crystallization. The lamellar PCL had lower crystallinity than the spherulitic PCL. The crystallinity further decrease with the decrease of nominal PCL layer thickness when PCL layers broke up into nanosheets and nanodroplets. The reduction of crystallinity resulted from less nucleation sites for heterogeneous nucleation crystallization in the PCL nanosheets and nanodroplets. Combining the WAXS analysis with the DSC analysis, the PCL nanosheets and nanodroplets

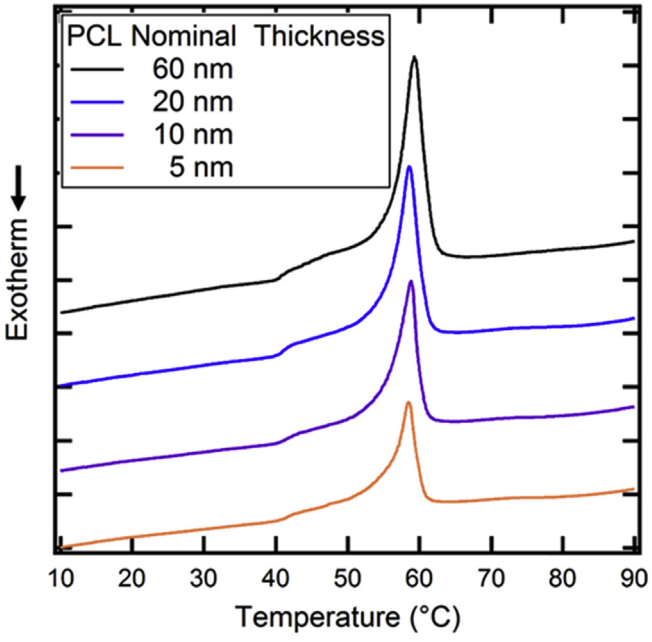

Fig. 10. DSC heating thermograms of 513 layer PS/PCL as-extruded films. The heating rate was 10 °C/minute. The heat flow was normalized to 100% PCL.

Table 3
PCL melting temperature and crystallinity measured by DSC, and the Hermans orientation function of PCL f_{110} analyzed from the azimuthal intensity distribution in the WAXS pattern.

PCL Nominal Thickness (nm)	T_m (°C)	Normalized Enthalpy of PCL Melting (J/g)	Crystallinity (%)	f_{110}
60	60	54 ± 5	40 ± 4	0.80
20	58	50 ± 5	37 ± 4	0.55
10	58	47 ± 5	35 ± 4	0.22
5	58	40 ± 4	30 ± 4	0.12

formed during coextrusion had lower crystallinity and reduced in-plane orientation compared with PCL layers.

4. Conclusions

The breakup behavior of PMMA nanolayers in the PS/PMMA system and PCL nanolayers in the PS/PCL multilayer films had been systematically studied. The onset for the appearance of breakups in the layers was identified in both cases for nominal thicknesses of 30–40 nm. The cross-sectional AFM images showed that when the nominal layer thicknesses below this value were targeted, some of the continuous layers started to lose continuity and developed into nanosheets. The number of continuous layers decreased and the number of nanosheets and nanodroplets increased with decreasing nominal layer thickness. As this process continued, the nanosheets then coalesced into nanodroplets with a further decrease of nominal layer thickness.

We also found that oxygen permeability was an effective probe efficiently to characterize layer breakup behavior in both semi-crystalline and glassy nanolayer systems. The threshold of oxygen permeability increase indicated the onset for layer breakup and traced the effect of nominal layer thickness on the degree of breakup. In terms of the glassy/glassy PS/PMMA system, the effective PMMA oxygen permeability remained constant when both PS and PMMA layers were continuous. The effective PMMA oxygen permeability started to increase when the layer thickness was below the onset for breakup and kept increasing until all PMMA layers broke up into nanosheets and nanodroplets. In terms of the glassy/semi-crystalline PS/PCL system, the evolution of the effective PCL oxygen permeability was more complex. It decreased at first due to confined crystallization of PCL with PS confinement. The crystallization orientation of PCL changed from spherulites to in-plane lamellae when the PCL layers thickness reached 100 nm causing the improvement of oxygen barrier properties. The oxygen permeability remained constant when the morphology of the PCL layer changed from stacked lamellae to single crystal lamellae. With the decrease of the PCL layer thickness, the PCL layers started to breakup into nanosheets and nanodroplets causing the increase in oxygen permeability. The breakup phenomena of the two systems were similar in terms of critical thickness and trend of increasing oxygen permeability. The increased oxygen permeability of the PS/PCL system during layer breakup was successfully modeled. Combining oxygen permeability measurements and atomic force microscopy, one could estimate and calculate the proportion of continuous PCL layers, nanosheets and nanodroplets. Wide-angle X-ray scattering and optical transmission could well predict the crystal orientation and domain size in PCL nanosheets and nanodroplets. The PCL nanodroplets were semicrystalline and did not have strong orientation compared to PCL continuous layers.

Layer breakup during the multilayer coextrusion process was proven to be a promising technique to produce nanoscaled polymer blends. Polymers could be selected from most polymer pairs ranging from amorphous materials and semicrystalline materials as long as they were coextrudable and had low miscibility. The nanodroplets of the minor phase were well dispersed in the polymer matrix. And finally, the domain size of the nanodroplets or nanoblends could be controlled by using different numbers of layer multiplication elements and changing the composition of the materials.

Acknowledgement

This research was generously supported by National Science Foundation under Grant No. DMR 0423914.

References

[1] W. Schrenk, Method for Multilayer Coextrusion, 1973. U.S. Patent 3773882.
[2] D. Langhe, M. Ponting, Manufacturing and Novel Applications of Multilayer Polymer Films, William Andrew, 2016.
[3] M. Gupta, Y. Lin, T. Deans, E. Baer, A. Hiltner, D.A. Schiraldi, Structure and gas barrier properties of poly (propylene-graft-maleic anhydride)/phosphate glass composites prepared by microlayer coextrusion, Macromolecules 43 (9) (2010) 4230–4239.
[4] C.-Y. Lai, A. Hiltner, E. Baer, L.T. Korley, Deformation of confined poly (ethylene oxide) in multilayer films, ACS Appl. Mater. Interfaces 4 (4) (2012) 2218–2227.
[5] Y. Jin, H. Tai, A. Hiltner, E. Baer, J.S. Shirk, New class of bioinspired lenses with a gradient refractive index, J. Appl. Polym. Sci. 103 (3) (2007) 1834–1841.
[6] T. Kazmierczak, H. Song, A. Hiltner, E. Baer, Polymeric one-dimensional photonic crystals by continuous coextrusion, Macromol. Rapid Commun. 28 (23) (2007) 2210–2216.
[7] K. Yin, Z. Zhou, D.E. Schuele, M. Wolak, L. Zhu, E. Baer, Effects of interphase modification and biaxial orientation on dielectric properties of poly (ethylene terephthalate)/poly (vinylidene fluoride-co-hexafluoropropylene) multilayer films, ACS Appl. Mater. Interfaces 8 (21) (2016) 13555–13566.
[8] E. Baer, L. Zhu, 50th anniversary perspective: dielectric phenomena in polymers and multilayered dielectric films, Macromolecules 50 (6) (2017) 2239–2256.
[9] Z. Qiang, J. Xue, K.A. Cavicchi, B.D. Vogt, Morphology control in mesoporous carbon films using solvent vapor annealing, Langmuir 29 (10) (2013) 3428–3438.
[10] Y. Zhu, A. Bironeau, F. Restagno, C. Sollogoub, G. Miquelard-Garnier, Kinetics of thin polymer film rupture: model experiments for a better understanding of layer breakups in the multilayer coextrusion process, Polymer 90 (2016) 156–164.
[11] H. Wang, J.K. Keum, A. Hiltner, E. Baer, Confined crystallization of PEO in nanolayered films impacting structure and oxygen permeability, Macromolecules 42 (18) (2009) 7055–7066.
[12] R. Adhikari, V. Seydewitz, K. Löschner, G.H. Michler, A. Hiltner, E. Baer, Structure and properties of multilayered PET/PC composites, Macromolecular Symposia 294 (1) (2010) 156–165.
[13] S. Scholtyssek, R. Adhikari, V. Seydewitz, G.H. Michler, E. Baer, A. Hiltner, Evaluation of morphology and deformation micromechanisms in multilayered PP/PS films: an electron microscopy study, Macromolecular symposia 294 (1) (2010) 33–44.
[14] A. Bironeau, T. Salez, G. Miquelard-Garnier, C. Sollogoub, Existence of a critical layer thickness in PS/PMMA nanolayered films, Macromolecules 50 (10) (2017) 4064–4073.
[15] T. Bernal-Lara, R. Liu, A. Hiltner, E. Baer, Structure and thermal stability of polyethylene nanolayers, Polymer 46 (9) (2005) 3043–3055.
[16] Y. Jin, A. Hiltner, E. Baer, R. Masirek, E. Piorkowska, A. Galeski, Formation and transformation of smectic polypropylene nanodroplets, J. Polym. Sci. B Polym. Phys. 44 (13) (2006) 1795–1803.
[17] Y. Jin, A. Hiltner, E. Baer, Fractionated crystallization of polypropylene droplets produced by nanolayer breakup, J. Polym. Sci. B Polym. Phys. 45 (10) (2007) 1138–1151.
[21] D.S. Langhe, J.K. Keum, A. Hiltner, E. Baer, Fractionated crystallization of α-and β-nucleated polypropylene droplets, J. Polym. Sci. B Polym. Phys. 49 (2) (2011) 159–171.
[23] M. Ponting, Y. Lin, J.K. Keum, A. Hiltner, E. Baer, Effect of substrate on the isothermal crystallization kinetics of confined poly (ε-caprolactone) nanolayers, Macromolecules 43 (20) (2010) 8619–8627.
[24] J.M. Carr, D.S. Langhe, M.T. Ponting, A. Hiltner, E. Baer, Confined crystallization in polymer nanolayered films: a review, J. Mater. Res. 27 (10) (2012) 1326–1350.
[25] J. Feng, G. Zhang, K. MacInnis, A. Olah, E. Baer, Formation of microporous membranes by biaxial orientation of compatibilized PP/Nylon 6 blends, Polymer 123 (2017) 301–310.
[26] Y. Jin, M. Rogunova, A. Hiltner, E. Baer, R. Nowacki, A. Galeski, E. Piorkowska, Structure of polypropylene crystallized in confined nanolayers, J. Polym. Sci. B Polym. Phys. 42 (18) (2004) 3380–3396.
[27] P.H. Hermans, Contribution to the Physics of Cellulose Fibres, Elseview Publishing Company, Iinc., London, 1946.
[28] H. Kweon, M.K. Yoo, I.K. Park, T.H. Kim, H.C. Lee, H.-S. Lee, J.-S. Oh, T. Akaike, C.-S. Cho, A novel degradable polycaprolactone networks for tissue engineering, Biomaterials 24 (5) (2003) 801–808.